# Journal of Materials Chemistry C

Accepted Manuscript


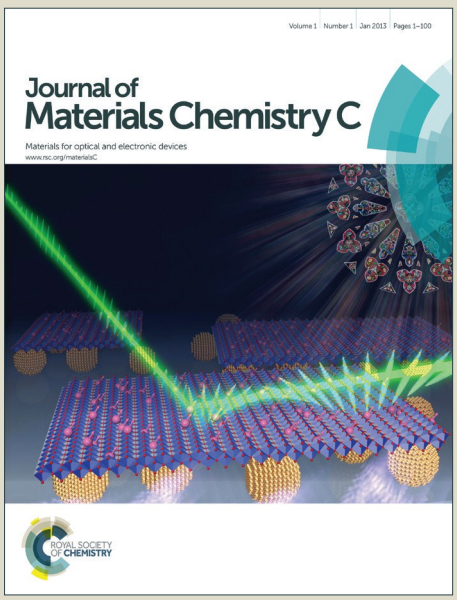





ROYAL SOCIETY OF CHEMISTRY

www.rsc.org/materialsC

Journal Name

ARTICLE

# High Transparency in the Structural Color Resin Films through Quasi-Amorphous Arrays of Colloidal Silica Nanospheres

Received 00th January 20xx,
Accepted 00th January 20xx

DOI: 10.1039/x0xx00000x

www.rsc.org/

Chun-Feng Lai,*[a] Yu-Chi Wang,[a] and Hsiang-Chih Hsu[a]

Periodic crystals are angle-dependent structures that typically exhibit iridescent colors, thus limiting their practical application. Consequently, uniform structural colors have substantial potential for use in optical devices. This paper presents a simple and inexpensive method for fabricating novel structural color resin films with high optical transparency, uniform reflection color, and physical rigidity. Quasi-amorphous resin films were fabricated through a molding process because of the shear-induced order and polymerization caused by the formation of quasi-amorphous structures trapped inside the polymer resin. A low index difference between colloidal silica nanospheres and the polymer resin led to the high transparency of composite resin films and uniform weak reflection colors. The reflectance spectra of the silica nanospheres showed reflection peaks from the ultraviolet to near-infrared regions depending on the nanosphere size. Angle-resolved reflection and scattering spectrometry results showed that the structural color of the sample originated from the constructive interference of quasi-amorphous structures. In addition, we demonstrated the quasi-amorphous resin films as novel optical filters for developing the white light-emitting diodes (WLEDs). This study successfully developed a novel technique can be applied in optical devices such as displays, sensors and WLEDs.

## Introduction

Colors in the biological world have two major sources, pigments and photonic structures. Pigmentary colors are known as chemical colors, and colors originating from photonic structures are considered physical colors. Compared with pigmentary colors, structural colors have many advantages, such as resistance to fading and environmental friendliness, leading to potential applications in various fields such as decoration and anticounterfeiting. Structural colors are widely observed in biological organisms and can be divided into two categories: iridescent color (angle dependent) from periodic structures such as butterfly wings[1–4] and non-iridescent color (angle independent) from amorphous structures (short-range ordered but long-range amorphous) such as blue-crowned Manakin (*Lavigeria coronata*) and plum-throated Cotinga (*Cotinga maynana*) feathers[5-7]. Iridescent color is generally angle dependent, limiting its application in optical devices such as displays, which require broad viewing angles[8]. Conversely, angle-independent colors remain unchanged regardless of the viewing angle and thus have considerable potential for use in optical devices such as sensors[9].

The self-assembly of monodisperse colloidal nanospheres forming periodic structures has been demonstrated using relatively simple and economical methods[10–14]. Colloidal crystals have poor adhesion and white structural color. Therefore, colloidal nanospheres embedded in polymer resins and polymer nanocomposites have been demonstrated to have wide applications such as displays, e-paper, and white light-emitting diodes (WLEDs)[15–17]. Many studies have reported fabricating angle-independent structural colors[18–22]. Takeoka (2010) mixed various submicron-sized silica nanospheres to prepare colloidal amorphous structures[19]. Takeoka (2013)[21] and Yang (2014)[22] were used spray-coated uniform silica nanospheres to fabricate colloidal amorphous and quasi-amorphous structures, respectively. In this study, we report a simple and manipulable method for fabricating highly transparent quasi-amorphous structural color resin films by combining colloidal silica nanosphere suspensions with a photocurable resin. We used nonuniform silica nanospheres dispersed in a photocurable resin to form quasi-amorphous structures through the shear-induced crystallization of the colloids and solidification enabled by ultraviolet (UV) photopolymerization. We prepared composite resin films with high transparency and uniform reflection color. The reflection color of the composite resin films was observed and tuned by varying the size of the silica nanospheres and the

[a] Department of Photonics, Feng Chia University, No. 100, Wenhwa Road, Seatwen, Taichung 40724, Taiwan. E-mail: chunflai@fcu.edu.tw

†Electronic Supplementary Information (ESI) available: Tables show the $NH_4OH$ volume for different sizes of silica nanospheres. The diffraction patterns of the samples were captured using a laser. The reflectance and transmittance spectra of the samples were measured at different incident angles. The effect of the guided light and the optical characteristics of the WLED bulbs were measured. See DOI: 10.1039/x0xx00000x

concentration of the colloidal silica suspensions. According to angle-resolved reflection, scattering, and transmission spectrometry, we deduced that the structural color originated from the constructive interference of light from the quasi-amorphous structures. In addition, a low refractive index difference resulted in high transmittance, providing high selectivity for various optical applications such as optical filters. In practice, this technique enables fabricating composite resin films with a large area and a controllable thickness.

## Experimental section

### Materials

Tetraethoxysilane (TEOS, 98%; Seedchem), ammonium hydroxide ($NH_4OH$, 28%; SHOWA), anhydrous ethanol (99.5%; Echo Chemical Co.), ethoxylated trimethylolpropane triacrylate (ETPTA, Mn = approximately 428; Sigma-Aldrich) as a monomer, and a photoinitiator, 2-hydroxy-2-methyl-1-phenyl-1-propanone (HMPP, Darocur 1173; Ciba Specialty Chemical), were used as received. Deionized (DI) water was purified using the PURELAB purification system.

### Synthesis of monodispersed silica nanospheres with a high polydispersity index

Monodisperse silica nanospheres of various sizes were synthesized by combining a titration method with the Stöber–Fink–Bohn method for growing the nanospheres. For example, to synthesize silica nanospheres with a mean diameter ($D_{mean}$) of 92 nm, anhydrous ethanol (100 mL), DI water (80 mL), and $NH_4OH$ (7 g) were mixed through magnetic stirring (600 rpm) in an Erlenmeyer flask, which was warmed in a water bath at 40 °C. After stirring for 4 h, TEOS (20 mL) was added to the reaction mixture by using a peristaltic pump (0.8 rpm). A peristaltic pump with a constant flow rate fed the TEOS into the reactor containing DI water, anhydrous ethanol, and $NH_4OH$. Table S1 lists the synthesis parameters, including the desired silica nanosphere size. After a 4 h reaction, the silica nanosphere powders were collected through centrifugation at 7000 rpm for 1 h and purified three times in an anhydrous ethanol wash before being dried in a convection oven.

### Preparation of colloidal silica-ETPTA resin suspensions

Five silica nanosphere powders with different weights were synthesized (samples A–E, Table S1) and dispersed in 2 g of ethanol at concentrations of 10, 20, and 30 weight percentage (wt%) by using ultrasonication (1200 W) for 8 h to ensure complete dispersion. The colloidal silica suspensions were then mixed with 1 g of ETPTA resin containing 1 wt% HMPP[16]. After mixing, the colloidal silica–ETPTA resin suspensions were ultrasonicated for 4 h to ensure dispersion. Finally, the ethanol in the mixing suspensions was completely evaporated by heating the solutions at 70 °C in a convection oven for 12 h. The final colloidal silica–ETPTA resin suspension concentrations were 18, 33, and 46 wt% (Media 1).

### Characterization

A peristaltic pump (SH-P100) with a pump head (SH-P15X) was used to synthesize the silica nanospheres (Shishin Tech. Co.). The morphologies of the colloidal silica–ETPTA resin films were observed using field-emission scanning electron microscopy (FESEM, S-4800; Hitachi). The silica nanosphere size distribution was determined using a laser particle size analyzer (LPSA, N4 plus; Beckman Coulter). An oxygen plasma etch of inductively coupled plasma (ICP; SPTS Multiplex ICP) was used for etching the polymerized ETPTA to release the silica nanospheres. The reflectance and transmittance of the colloidal silica–ETPTA resin films were measured using a UV–Visible spectrometer (HR2000 + CG–UV–VIS–NIR; Ocean Optics) with an optical resolution of 1.0 nm and were calculated using SpectraSuite software (Ocean Optics). The angle-resolved reflection, scattering, and transmission optical setups contained collected light from a CP140 spectrophotometer with a Sygnature charge-coupled device detector (Jobin Yvon; Horiba); a fiber-coupled UV-enhanced Xe lamp was used as a white light source, and a double-motorized rotation stage collected light as a function of the zenith angle with a resolution of 1°. A reflection-mode optical microscope (BXFM; Olympus) with a color digital camera (uEye LE; iDS) was used to observe the edge emission of the colloidal silica–ETPTA resin films. Diffraction patterns were captured by using a He–Ne laser ($\lambda$ = 632 nm; JDS Uniphase Corp.) The optical characteristics of WLED bulbs were measured by using a 20-in integration sphere with a radiometer and photometer (SC-610; Labsphere).

### Supporting Video Clip

A video clip of the viscosity effect exhibited during sample B and sample C (Media 1). A real-time video clip of the light-guided phenomenon that occurred as the colloidal silica–ETPTA resin films transmitted the incident light of the light source was obtained using an iDS digital camera (Medias 2 and 3).

## Results and discussion

### Quasi-amorphous structures of the fabricated colloidal silica-ETPTA resin films

A previous study demonstrated the fabrication of monodisperse silica nanospheres through the controlled hydrolysis of TEOS in ethanol, followed by the condensation of the dispersed phase material[23]. Previous studies have demonstrated a polydispersity index (PI) lower than 0.05 that formed periodic crystals, which were synthesized using the revised Stöber–Fink–Bohn method[24–26]. To obtain a PI of silica nanospheres higher than 0.05 that could form quasi-amorphous structures, we used a titration method to control the hydrolysis and condensation and a high DI water concentration to increase the velocity of the hydrolysis[27]. In this study, the PIs of the silica nanospheres formed using the titration method were higher than 0.05 according to the dynamic light scattering measurement performed using a LPSA;

the results are listed in Table S1 and Figure S1. In addition, we increased the $NH_4OH$ concentration to obtain a large nanosphere size (Table S1).

To elucidate the nanosphere arrangement of the colloidal silica-ETPTA resin films, the ETPTA polymer resins were etched using an etching method of oxygen ICP[28,29] at an oxygen pressure of 140 mTorr, an oxygen flow rate of 50 sccm, an argon flow rate of 5 sccm, and a coil/platen working power of 5 W/10 W for 120 s before the embedded colloidal silica nanospheres were released. The results were observed using FESEM (Fig. 1). This treatment resulted in the partial removal of the ETPTA polymer surface and the exposure of the top array of silica nanospheres. Top-view and cross-sectional FESEM images (sample B) depicted short-range ordered and long-range amorphous structures, such as that seen in *C. maynana* feathers[5-7]. Similar structures can be obtained using this method. In addition, the diffraction pattern of sample C (Fig. S2) was a circular ring pattern, suggesting that the colloidal silica–ETPTA resin films were isotropically distributed with short-range ordered structures, a result consistent with FESEM outcomes. Therefore, the uniform structural color was attributed to the isotropic nature of the assemblies of the quasi-amorphous structures.

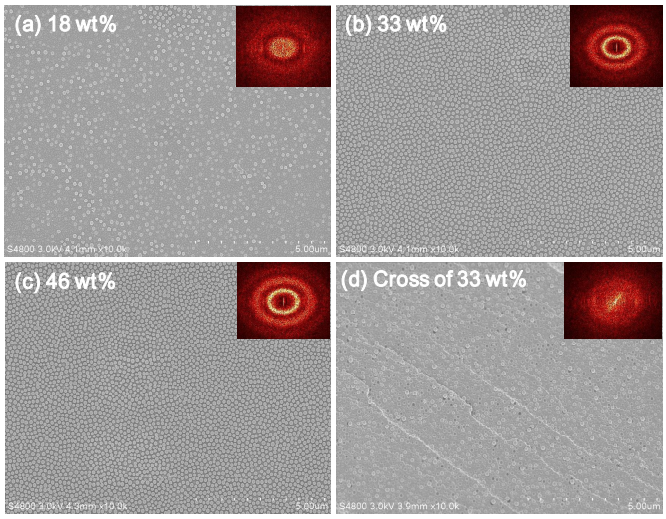


Figure 1. FESEM images of colloidal silica–ETPTA resin films with concentrations of (a) 18 wt%, (b) 33 wt%, and (c) 46 wt% and a mean silica nanosphere diameter of 92 nm (sample B). (d) Cross-sectional FESEM images of sample B. Short-range ordered and long-range amorphous structures are evident from fast Fourier transformation images (insets).

Transparent colloidal silica–ETPTA resin films of varying areas were prepared through a molding process involving a quartz mold with a 250 μm notch and various diameters (Fig. 2). Figure 2(a) shows the color of the colloidal silica–ETPTA resin suspension after the ethanol evaporated. Next, the colloidal silica–ETPTA resin suspension was added to the mold notch, which was covered by glass and exposed to UV light through a high-intensity discharge lamp (HPA 400/30 S; Philips) for 5 min. The polymerized solidified resin films were separated from the mold carefully. In this study, the viscosity of silica-ETPTA resin suspensions depended on the concentration of silica nanosphere suspensions. We concluded the structural color resin films with quasi-amorphous structures that have been successfully fabricated using this method even though the high viscosity of the ETPTA resin suspensions, which leads to the formation of a crystalline structure in the suspension that is robust to disturbances from flows or Brownian diffusion[30,31]. In addition, the refractive index of silica nanospheres is the same as that of the highly polar ETPTA medium, and thus they spontaneously organize into an ordered phase[16]. Figure 2(b) shows an optical photograph of the colloidal silica–ETPTA resin films of various nanosphere sizes fabricated through the molding process. The composite resin films exhibited high transparency and uniform shining structural color caused by the constructive interference of light from the short-range ordered quasi-amorphous structures.

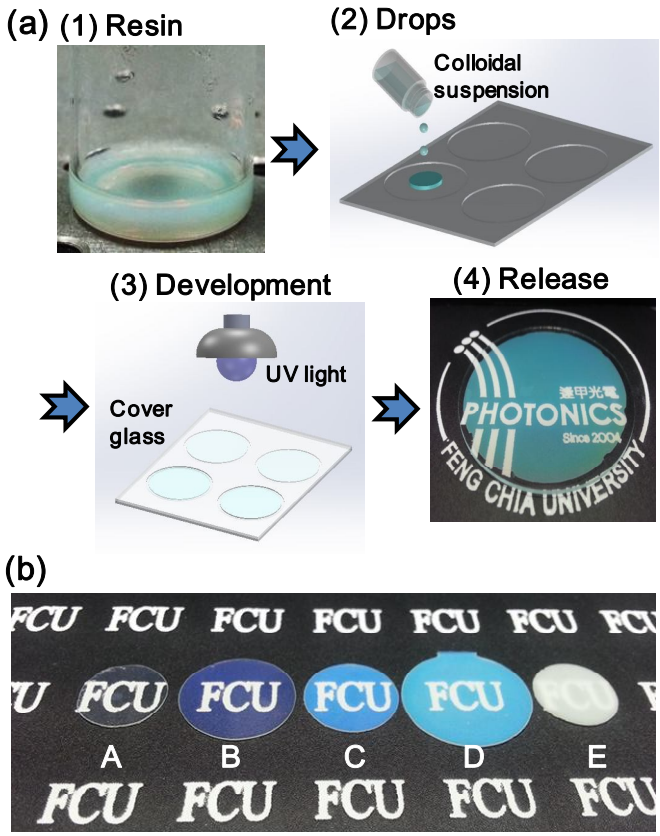


Figure 2. (a) Schematic of the molding process used to prepare the quasi-amorphous composite resin films. Step 1: Green colloidal silica–ETPTA resin suspension at a concentration of 33 wt% (sample C). Step 2: Addition of the colloidal silica–ETPTA resin suspension into a quartz mold notch. Step 3: Exposure of the colloidal silica–ETPTA resin suspension to UV light through a cover glass. Step 4: Careful release of the polymerized disk films from the quartz mold. (b) Optical photography images of composite resin films with different structural colors fabricated using a 46 wt% colloidal silica–ETPTA resin suspension with mean nanosphere diameters of 73 nm (A), 92 nm (B), 176 nm (C), 196 nm (D), and 236 nm (E) on black kraft paper under room lighting.

The molding process described here has several advantages. First, it is rapid, inexpensive, and highly manipulable. Planar glass (diameter = 2.5 in.; Fig. 2(a)) can be fabricated in a few minutes. Second, a wide nanosphere diameter range can be achieved using this process. The formation of cracks can be completely avoided in the short molding process and photopolymerization time. According to the Bragg–Snell law, reflection light is tuned by adjusting the nanosphere concentrations and sizes, respectively. For instance, we used 176 nm (average) silica nanospheres (sample C), and the composite resin films exhibited green and blue colors at concentrations of 33 and 46 wt%, respectively (Figs. 2(a) and 2(b)). This phenomenon was also observed in a different sample.

## Optical properties of colloidal silica-ETPTA resin films

The quasi-amorphous structures of highly transparent silica-ETPTA resin films were fabricated using a photocurable ETPTA resin ($n_{ETPTA}$ = 1.469) as a dispersion medium for embedded silica nanospheres ($n_{silica}$ = 1.45)[16]. In our experiments, colloidal silica nanospheres were formed with quasi-amorphous structures because the PI value was greater than 0.05. In addition, we prepared periodic structures of colloidal silica–ETPTA resin films with a PI lower than 0.05 with similar results to those reported previously[15,16]. As illustrated in Figs. 2(b) and 3(a), the uniform structural color resin films, depending on the sizes of the silica nanospheres and the suspension concentrations, reflected light in the UV–near-infrared (NIR) region, a result observed in silica nanospheres with mean diameters of 70–240 nm. To characterize the structural color and to elucidate the reflection and transmission colors (Figs. 3(a) and S3), we measured the reflectance and transmittance of 33 wt% silica–ETPTA resin films with mean silica nanosphere diameters of 70 (A)–240 nm (E) (Figs. 3(c) and 3(d)). Distinct weak peaks were observed at approximately 413 (B), 550 (C), 570 (D), and 711 nm (E), which were attributable to the constructive interference of the reflection light from the quasi-amorphous structures of nanospheres with different sizes[21,22], which are discussed more fully in the next section. Despite the difference in the refractive index being small, the colloidal silica–ETPTA resin films exhibited significant surface reflection and high transparency; the high transparency can be used to control the resin film thickness. In addition, we clearly read the term "*ASODL*" under a fluorescent lamp when it was covered by the composite resin films. Figure 3(d) shows the normal incident transmittance of composite resin films, which exhibit approximately 90% transmittance for wavelengths longer than the reflection wavelengths and 30% transmittance for shorter wavelengths, further illustrating the reflection color, transmission color, and transparency of the composite resin film (Fig. 3(a)). Furthermore, an analysis of the effects of the colloidal silica–ETPTA resin suspension concentration (sample C; Fig. S3) showed that reducing the concentration caused a red-shifted reflection peak in the reflectance spectra which led to changes in the volume-filling fractions of three nanosphere concentrations on the top surface of the nonpacking silica nanosphere structures of the composite resin films (FESEM images; Fig. 1).

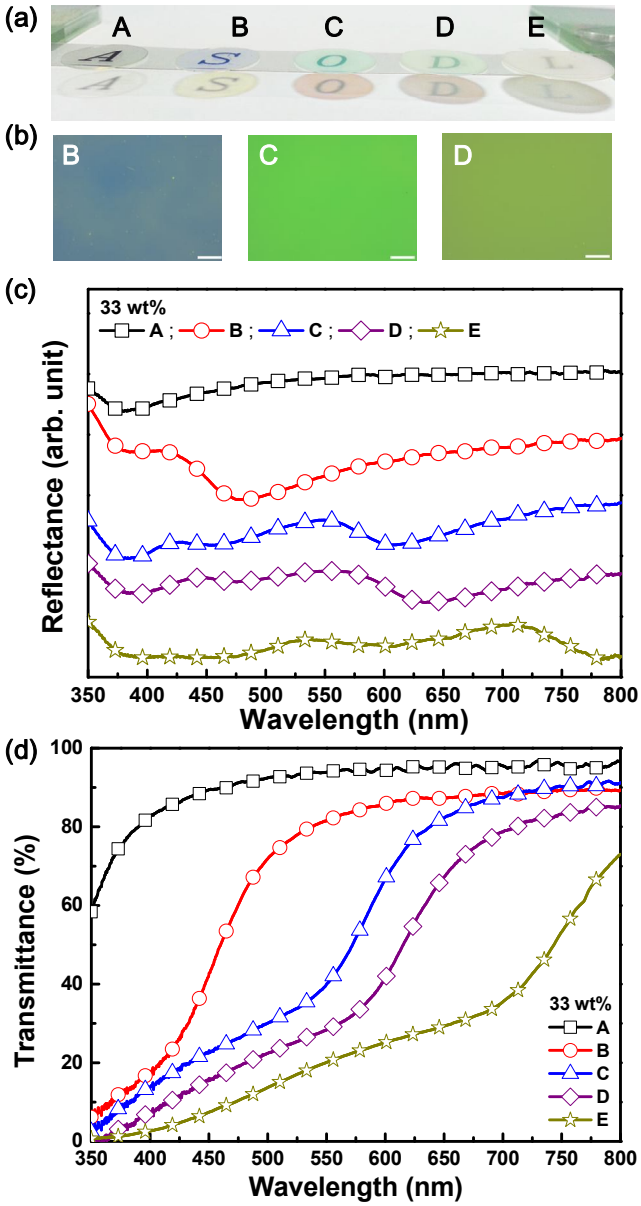


Figure 3. (a) Optical photography images of the reflection and transmission colors of colloidal silica–ETPTA resin films of 33 wt% (samples A–E). (b) Three sets of optical microscopy images of colloidal silica-ETPTA resin films operated in dark-field mode. (scale bar = 50 μm) (c) Reflectance and (d) transmittance of the colloidal silica–ETPTA resin films with different nanosphere diameters.

The transmission light distribution of the composite resin films was evaluated using an angle-resolved transmittance technique[17,32,33]. The angle-resolved transmittance spectra as a function of the detection angle $\gamma$ were recorded using a fiber probe coupled to an optical spectrometer. A motorized rotation stage connected to the optical spectrometer was rotated from $\gamma = 0°$ (normal) to 70° in increments of 1.0°, and a fiber-to-sample distance of 15 cm was maintained. The transmittance spectra were displayed on a plot of wavelength

versus detection angle, with the color indicating the transmittance. Figure 4(a) shows the transmittance spectra recorded in unpolarized light for composite resin films of sample B (46 wt%). The transmittance measurement results showed that as the $\gamma$ detection angle was increased, the transmission wavelength shifted slightly toward longer wavelengths (Fig. 4(b)) which contributed to the uniform color of the composite resin films.

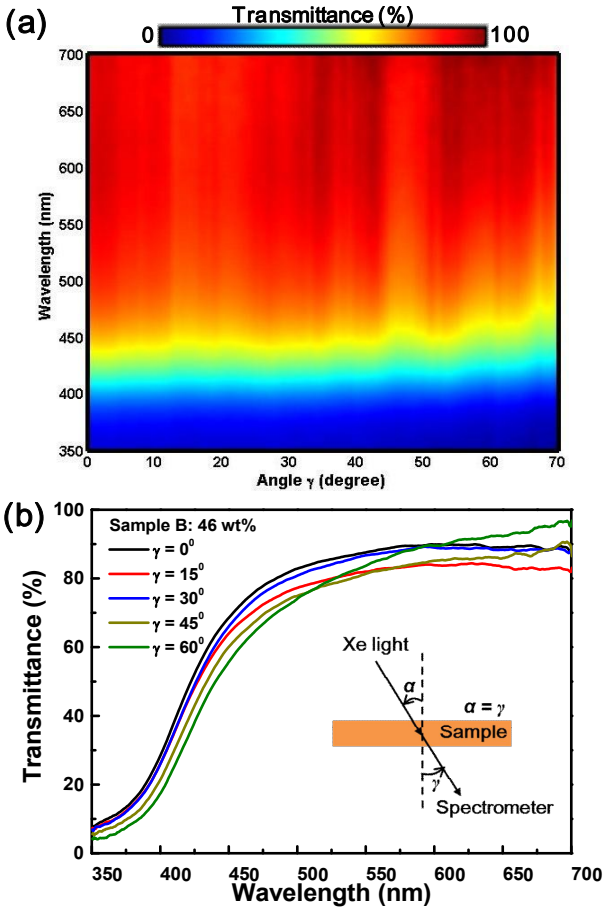


Figure 4. (a) Angle-resolved transmittance spectra of colloidal silica–ETPTA resin films (sample B, 46 wt%). (b) Transmittance spectra at selected detection angles. The spectra are sections of the angle-resolved transmittance map along the detected angle.

## Reflection color generation involving constructive interference

To investigate the angle dependence of structural colors, specular reflection, near-backward scattering, and diffusive scattering should be evaluated[7]. Therefore, we demonstrated the angle-resolved reflection and scattering spectra to fully characterize the structural color of the colloidal silica–ETPTA resin films. The angle-resolved experimental setup was based on Ref. 7. A sample was mounted at the rotation center of a rotation stage as goniometer. Collimated broadband white light from a UV-enhanced Xe lamp was incident on the sample at an angle $\alpha$ from the surface normal, in which the ETPTA resin film as reference for the reflectance measurement was the incident light of the Xe light source. The light spot size on the sample was about 4.0 mm. Reflected or scattered light was collected by a lens and focused to an optical fiber that was connected to a spectrometer. First, the angle-resolved specular reflection was measured in the $\alpha$-2$\alpha$ geometry, that experimental setup shown inset Fig. 5(b). We fixed the incident arm, and rotated the sample and the detect arm[7], with angle $\alpha$ changing from 10° to 50° as the sample rotated. Figures 5(a) depicts the color maps showing the reflected intensity as function of the incident angle $\alpha$ and reflection wavelength $\lambda_R$ for sample C (33 wt%). The angle-resolved specular reflection spectral behavior of quasi-amorphous composite resin films was similar to that of the ordered periodic structures (Figs. 5(a) and S4)[19–22,33]. The blue-shifted reflection peak of the quasi-amorphous structures with increasing $\alpha$ was indicated the structural colors generated by quasi-ordered structures depend on angles of incidence[7].

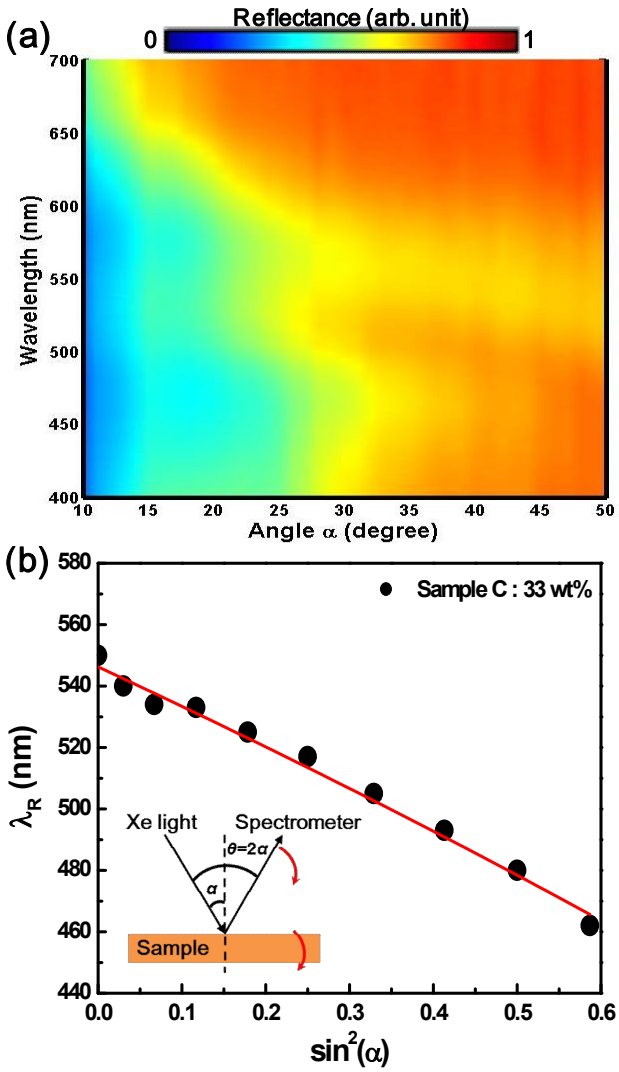


Figure 5. (a) Angle-resolved specular reflection measurement of composite resin films (sample C, 33 wt%). (b) The relationship between $\lambda_R$ and $sin^2(\alpha)$ from (a), where $\lambda_R$ is the reflection peak wavelength and the red line is the linear fitting. Inset: Schematic of the experimental setup, in which the red arrow represents the rotation direction.

The angle-resolved specular reflection spectra were used to demonstrate the structures. Figures 5(b) and S4 show the linear relationship between the reflection angle and the position of the reflection peak, indicating the contribution of the constructive interference to the reflection color[22]. As Figs. 5 and S4 show, when the incident angle, $\alpha$, was increased from 10° to 50°, the intensity of specular reflection increased, and this was accompanied by a blue-shift of the reflection peak. This phenomenon is similar to the observations of a periodic structure, except that the peaks were much broader and weaker than the periodic structure, suggesting that the reflected light was dominated by the constructive interference of light, and the short-range ordering considerably attenuated the reflected light[7,22]. The nanospheres were organized with a certain degree of ordering (a top-view FESEM image of the quasi-amorphous structures is shown in Fig. 1). The reflection peak of quasi-amorphous structures is believed to depend on the specular angle because of the constructive interference of light from the short-range ordered composite resin films. Moreover, the experimental data in Fig. 5(a) can be used to calculate the effective refractive index ($n_{eff}$) by using the Bragg–Snell law. We also calculated the volume filling fraction of colloidal silica-ETPTA resin films. First, the volume filling fraction ($f_{Silica}$) of silica nanospheres of 33 wt% silica-ETPTA resin film (sample C; $f_{Silica}$ = 0.1998) was calculated from the density of silica nanospheres[34] ($\rho_{Silica}$ = 2.22 g cm$^{-3}$) and ETPTA ($\rho_{ETPTA}$ = 1.11 g cm$^{-3}$). Then, the effective refractive index ($n_{eff}$) was obtained using eq. (1):

$$n_{eff}^2 = n_{Silica}^2 f_{Silica} + n_{ETPTA}^2 \left(1 - f_{Silica}\right) \qquad (1)$$

where $n_{Silica}$=1.45 and $n_{ETPTA}$=1.469[16]. In this study, we obtained $n_{eff}$ = 1.465 for the structural color resin film sample C (33 wt%). Next, according to the Bragg–Snell law (eq. (2)), the relationship between the reflection peak wavelength $\lambda_R$ and incident angle $\alpha$ of an ordered structure is

$$\lambda_R = 2d_{int}\sqrt{n_{eff}^2 - \sin^2\alpha} \qquad (2)$$

where $d_{int}$ is the interlayer spacing. A linear relationship was observed between $\lambda_R$ and $sin^2(\alpha)$ in the composite resin films (Fig. 5(b)), suggesting that the spectra of quasi-amorphous structures at reflection angles can be fitted using eq. (2). We obtained $d_{int}$ = 186.44 nm and $n_{eff}$ = 1.465 for the structural color resin film sample C (33 wt%) by using linear fitting. Finally, the $f_{Silica}$ of experimental results were consistent with the theoretical density calculation. The uniform structural color resin film in our system was clearly quasi-amorphous with both ordered and random structures.

Next, to measure the angle-resolved near-backward scattering spectra, we fix the detection arm and rotate only the sample[7], that experimental setup shown in Fig. 6(a). The angle $\vartheta$ between the incident arm and detection arm is kept at 20°, while the incident angle $\alpha$ changes from 10° to 60° with sample rotation. Figure 6(a) shows the measured backward scattering intensity (sample D, 46 wt%) as function of $\alpha$ and wavelength. As $\alpha$ increases, the specularly reflected light moves away from the detector. At larger $\alpha$ the detector collects the backward scattered light. As shown in Fig. 6(a), the spectral peaks remain for sample of colloidal silica–ETPTA resin films. These results indicates light is not only specular reflected, but also scattered into other directions. The peak wavelengths remain nearly constant as sample rotates. Thus the structural colors are independent of sample orientations, which is consistent with the isotropic nature of the quasi-ordered structures.

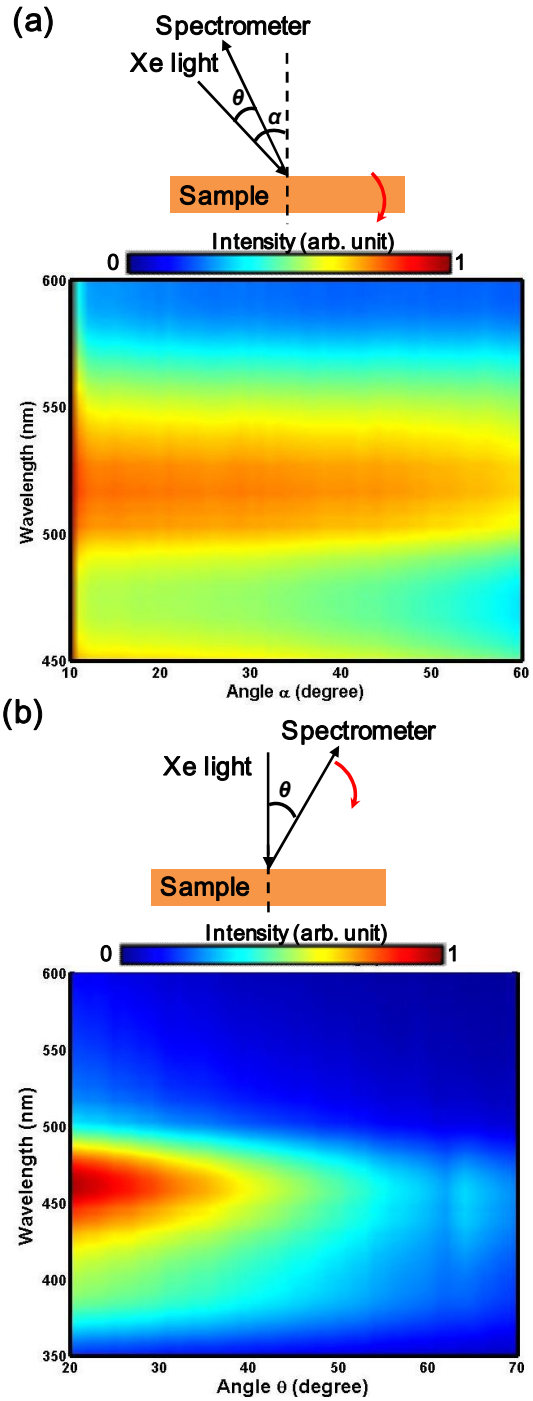


Figure 6. (a) Angle-resolved near-backward scattering spectra of composite resin films (sample D, 46 wt%). (b) Angle-resolved diffuse scattering spectra of composite resin films (sample B, 33 wt%). Top: Schematic diagrams of optical setups for measurement, in which the red arrow represents the rotation direction.

Finally, to measure the diffuse scattered light, we fix the sample and rotate only the detection arm[7], that experimental setup shown in Fig. 6(b). In this experiment, the incident angle of white light remains normal incidence, while the observation angle $\vartheta$ changes from 20° to 70°. Figure 6(b) shows the measured diffuse scattered intensity (sample B, 33 wt%) as function of $\vartheta$ and wavelength. The spectral peaks can be observed at all $\vartheta$, confirming light is scattered into all directions. However there is selectivity in the wavelength of scattered light, i.e., not all wavelengths are diffuse scattered with equal strength, leading to a peak in the diffuse scattering spectrum. The wavelength of diffuse scattering peak is no change with $\vartheta$, suggesting the color is independent on the observation angle.

Summary, for the quasi-amorphous structures, the reflected light intensity varies drastically with observation angle, but the scattered light intensity remains constant with observation angle. It demonstrates short-range order of quasi-amorphous structures is sufficient to produce structural color via constructive interference. The structural colors are invariant with the observation direction. This phenomenon can be understood as that the structure is isotropic and when illumination is also isotropic all directions of observation are equivalent[7].

## Guided light observed in colloidal silica-ETPTA resin films

As discussed we observed the propagation of approximately 10% of the transmittance light as it was guided from the silica–ETPTA resin films (Fig. 7). Figure 7(a) shows the experimental setup that was used to observe and measure the light-guided behavior, where $d_{Dist}$ is the distance between the Xe light source and the objective. The white light was normal incident on the middle ($d_{Dist}$ = 0 mm) of the composite resin films (samples B and C in Figs. 7(b) and 7(c), respectively), and two optical phenomena were observed: (1) The surface of the composite resin films exhibited violet (385 nm) and green (504 nm) reflection light, which matched the reflected peaks of the reflectance measurement in Fig. 7(d). (2) Guided yellow (578 nm) and red (717 nm) light, depending on the distance $d_{Dist}$, was observed on the edge of the composite resin films. The transmittance spectra are shown in Fig. 7(e). In this study, the guided light changed the wavelength of light from the composite resin films and caused the perception of relative motion of the light source relative to the observer (camera; Medias 2 and 3). The transmittance versus edge emission wavelength was measured depending on the distance $d$ from samples B and C (46 wt%; Fig. S5). As the light source was moved slowly nearer the objective, the edge emission wavelength showed the blue-shifted, as shown in Fig. 7(f). This study was the first to demonstrate these results for this optical phenomenon. Our results may prompt future studies to include more relation research.

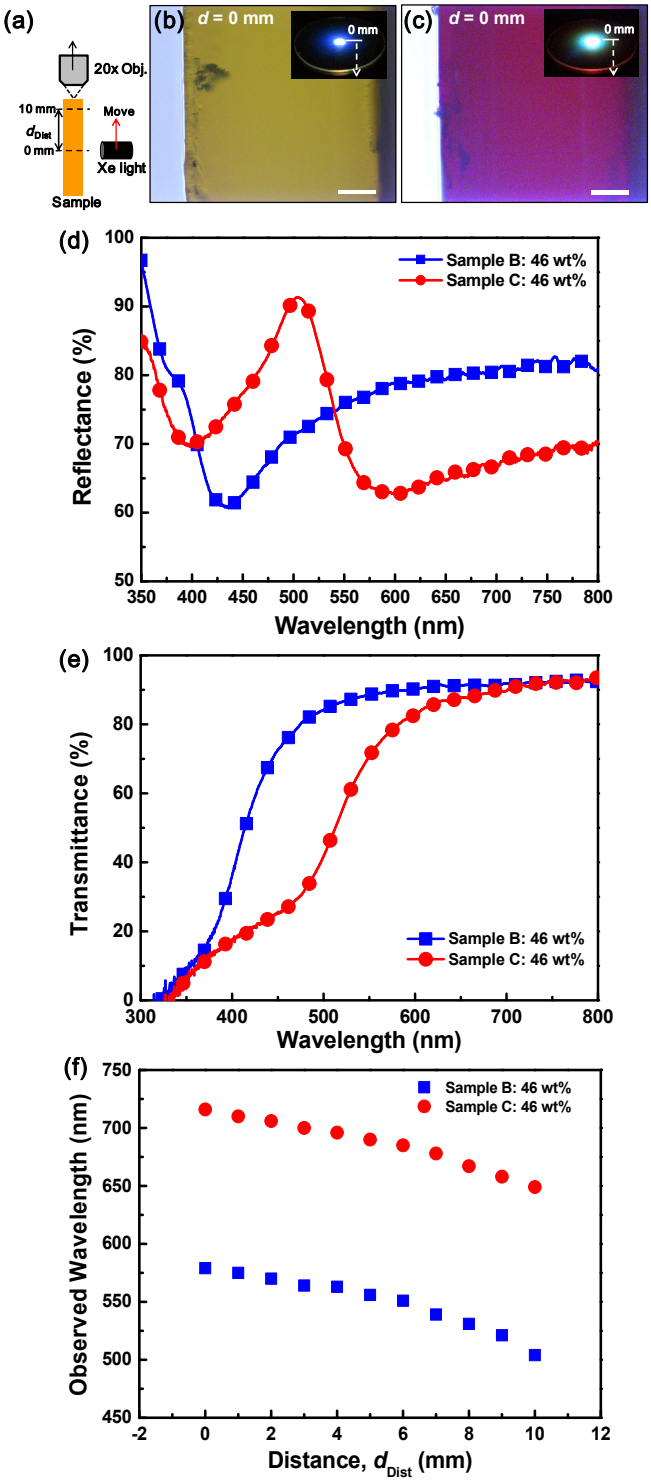


Figure 7. (a) Experimental setup for the guided light observed measurements, where $d_{Dist}$ is distance between Xe light source and objective, and "Obj." denotes "objective." (b) and (c) Optical photography images of the composite resin films (samples B and C, 46 wt%, respectively) that exhibited the edge emission color when the Xe light was incident in the middle ($d_{Dist}$ = 0 mm) of the sample. (scale bar = 50 μm) (d) Reflectance and (e) Transmittance of the colloidal silica–ETPTA resin films of samples. (f) Edge emission wavelength depends on the observed distance ($d_{Dist}$).

## Colloidal silica-ETPTA resin films application for WLED bulbs

In recent times, WLEDs have been used all over the world, because they can replace the energy inefficient incandescent bulbs and fluorescent lamps. Therefore, WLEDs have been a popular source of general illumination. The main strategy to fabricate WLEDs was usually used the phosphor-converted WLEDs. They are the most efficient method that provide high luminous efficiency and a low cost, but they used the most frequently phosphors of rare earth elements. In this study, the light emission spectrum of commercial WLED bulbs containing composite resin films was modified to resemble lower correlated-color temperature (CCT) of WLED bulbs.

We measured the luminous flux, luminous efficiency, CCT, and the International Commission on Illumination (CIE) color chromaticity coordinates (*x*, *y*) by using an integration sphere, at an operated power of 4.5 W. Table 1 lists the optical properties of four types of WLED bulbs. The CCT of WLED bulbs with composite resin film (sample C, 46 wt%) can decrease from approximately 6251 K to approximately 4407 K without increasing the yellow- and red-emitting phosphor powder. Therefore, this novel technology could reduce the fabrication cost of warm WLED bulbs.

Table 1. Optical characteristics of all WLED bulbs.

| Light source (@ 4.5 W) | Luminous flux (lm) | Luminous efficacy (lm/W) | CCT (K) | CIE coordinate (*x*, *y*) |
|---|---|---|---|---|
| LED bulbs | 365 | 81 | 6251 | (0.3183, 0.3202) |
| B film, 46 wt% | 363 | 81 | 5372 | (0.3354, 0.3468) |
| C film, 46 wt% | 360 | 80 | 4407 | (0.3688, 0.3907) |
| D film, 46 wt% | 338 | 75 | 4369 | (0.3684, 0.3819) |

In addition, the luminescence spectra of the WLED bulbs with and without composite resin films were measured by the integration sphere, as shown in Fig. S6. Due to the quasi-amorphous structures of composite resin films affect the luminescence spectrum of WLED bulbs. The CIE (*x*, *y*) coordinates define numerous standard illuminants that are used as colorimetric references. In this study, the CIE (*x*, *y*) coordinates of all four types of WLED bulbs were located near the Planckian locus of the CIE chromaticity diagram, as shown in Fig. 8. The experimental results indicated that the CCT and CIE (*x*, *y*) coordinates of the composite resin films deposited onto the tunable WLED bulbs depended on the sizes of silica nanospheres of the composite resin films. Figure 8 inset shows present photographs of the two light sources, WLED bulbs and WLED bulbs containing deposited composite resin films, respectively. The WLED bulbs containing composite resin films have several advantages. First, the CCT of WLEDs can be tunable by the varying silica-ETPTA resin films. Second, the surface of WLEDs is like the white color as tradition fluorescent lamp shell when the uniform structural color resin films deposited on the WLED bulbs. Therefore, using this novel technique helps reduce the use of phosphor powder in warm WLED bulbs.

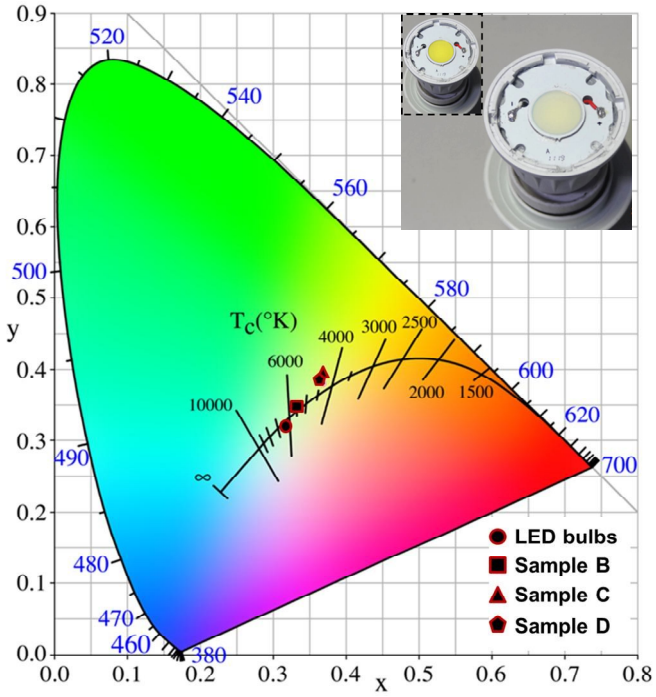


Figure 8. CIE color chromaticity coordinates (*x*, *y*) of four types of light sources. The inset shows a colloidal silica-ETPTA resin films placed on the LED bulbs.

## Conclusions

We experimentally demonstrated the fabrication of uniform structural color resin films with quasi-amorphous structures by using colloidal silica–ETPTA resin suspensions. The structural color was confirmed according to angle-resolved reflection, scattering, and transmission spectra. According to the measurement results, we confirmed that the structural color of the quasi-amorphous composite resin films originated from the constructive interference of reflection light from short-range ordered structures. The isotropic nature of quasi-ordered structures makes the colors uniform under natural light. We conclude that, by adjusting the sizes of the silica nanospheres and the suspension concentrations, the suggested fabrication method can be manipulated to create quasi-amorphous composite resin films with well-controlled volume-filling fractions. This method can be employed for designing color resin films with high transparency and different structural colors for use in potential applications such as windows, textiles, cosmetics, displays, sensors, and WLEDs.

## Acknowledgements

This work is supported by the Ministry of Science and Technology (MOST) in Taiwan, under contract numbers MOST102-2632-E-035-001-MY3, MOST103-2221-E-035-029, and MOST103-2622-E-035-007-CC2. The authors would like to thank Dr. Y. C. Chu at industrial technology research institute

(ITRI) in Taiwan support for oxygen plasma etch of ICP. The authors appreciate the Preci-sion Instrument Support Center of Feng Chia University in providing the fabrication and measurement facilities.

## Notes and references

1 M. Srinivasarao, *Chem. Rev.*, 1999, **99**, 1935–1961.
2 P. Vukusic, and J. R. Sambles, *Nature*, 2003, **424**, 852–855.
3 R. A. Potyrailo, H. Ghiradella, A. Vertiatchikh, K. Dovidenko, J. R. Cournoyer, and E. Olson, *Nat. Photonics*, 2007, **1**, 123–128.
4 F. Marlow, Muldarisnur; P. Sharifi, R. Brinkmann, and C. Mendive, *Angew. Chem. Int. Ed.*, 2009, **48**, 6212–6233.
5 J. F. Forster, H. Noh, S. F. Liew, V. Saranathan, C. F. Schreck, L. Yang, J. G. Park, R. O. Prum, S. G. J. Mochrie, C. S. O'Hern, H. Cao, and E. R. Dufresne, *Adv. Mater.*, 2010, **22**, 2939–2944.
6 Y. Takeoka, *J. Mater. Chem.*, 2012, **22**, 23299–23309.
7 H. Noh, S. F. Liew, V. Saranathan, S. G. J. Mochrie, R. O. Prum, E. R. Dufresne, and H. Cao, *Adv. Mater.*, 2010, **22**, 2871-2880.
8 H. Gu, Y. Zhao, Y. Cheng, Z. Xie, F. Rong, J. Li, B. Wang, D. Fu, and Z. Gu, *Small*, 2013, **9**, 2266-2271.
9 B. Ye, F. Rong, H. Gu, Z. Xie, Y. Cheng, Y. Zhao, and Z. Gu, *Chem. Commun.*, 2013, **49**, 5331-5333.
10 L. T. Varghese, Y. Xuan, B. Niu, L. Fan, P. Bermel, and M. Qi, *Adv. Optical Mater.*, 2013, **1**, 692-698.
11 L. Bai, Z. Xie, W. Wang, C. Yuan, Y. Zhao, Z. Mu, Q. Zhong, and Z. Gu, *ACS Nano*, 2014, **8**, 11094-11100.
12 C. Hu, Yi Chen, *Chem. Engin. J.*, 2015, **271**, 128-134.
13 H. Kang, J. S. Lee, W. S. Chang, and S. H. Kim, *Adv. Mater.*, 2015, **27**, 1282-1287.
14 Q. Fu, A. Chen, L. Shi, and J. Ge, *Chem. Commun.*, 2015, **51**, 7382-7385.
15 S. H. Kim, S. J. Jeon, G. R. Yi, C. J. Heo, J. H. Choi, and S. M. Yang, *Adv. Mater.*, 2008, **20**, 1649–1655.
16 H. S. Lee, T. S. Shim, H. Hwang, S. M. Yang, and S. H. Kim, *Chem. Mater.*, 2013, **25**, 2684–2690.
17 C. F. Lai, Y. C. Lee, and T. L. Tsai, *Opt. Mater. Express*, 2014, **5**, 307–313.
18 Y. Takeoka, M. Honda, T. Seki, M. Ishii, and H. Nakamura, *ACS Appl. Mater. & Inter.*, 2009, **1**, 982–986.
19 M. Harun-Ur-Rashid, A. B. Imran, T. Seki, M. Ishii, H. Nakamura, and Y. Takeoka, *ChemPhysChem*, 2010, **11**, 579–583.
20 K. Chung, S. Yu, C. J. Heo, J. W. Shim, S. M. Yang, M. G. Han, H. S. Lee, Y. Jin, S. Y. Lee, N. Park, and J. H. Shin, *Adv. Mater.*, 2012, **24**, 2375–2379.
21 Y. Takeoka, S. Yoshioka, A. Takano, S. Arai, K. Nueangnoraj, H. Nishihara, M. Teshima, Y. Ohtsuka, and T. Seki, *Angew. Chem.*, 2013, **125**, 7402-7406.
22 D. Ge, L. Yang, G. Wu, and S. Yang, *J. Mater. Chem. C*, 2014, **2**, 4395–4400.
23 W. Stöber, and A. Fink, *J. Colloid Inter. Sci.*, 1968, **26**, 62–69.
24 G. H. Bogush, M. A. Tracy, and C. F. Zukoski IV, *J. Non-Cryst. Solids*, 1988, **104**, 95–106.
25 P. Jiang, and M. J. McFarland, *J. Am. Chem. Soc.*, 2004, **126**, 13778–13786.
26 S. H. Kim, S. H. Kim, W. C. Jeong, and S. M. Yang, *Chem. Mater.*, 2009, **21**, 4993–4999.
27 H. S. Lee, J. H. Kim, J. S. Lee, J. Y. Sim, J. Y. Seo, Y. K. Oh, S. M. Yang, and S. H. Kim, *Adv. Mater.*, 2014, **26**, 5801–5807.
28 S. K. Park, K. D. Kim, and H. T. Kim, *Colloids Surf A Phys Engin Aspects*, 2002, **197**, 7–17.
29 C. Y. Cai, K. Y. A. Lin, and H. Yang, *Appl. Phys. Lett.*, 2014, **105**, 201913.
30 G. K. Batchelor, *J. Fluid Mechanics*, 1976, **74**, 1-29.
31 R. T. Foister, and T. G. M. Van De Ven, *J. Fluid Mechanics*, 1980, **96**, 105-132.
32 M. Muldarisnur, I. Popa, and F. Marlow, *Phys. Rev. B*, 2012, **86**, 024105.
33 C. F. Lai, Y. C. Lee, and C. T. Kuo, *J. Light. Tech.*, 2014, **32**, 1930-1935.
34 V. M. Masalov, N. S. Sukhinina, E. A. Kudrenko, and G. A. Emelchenko, *Nanotechnology*, **22**, 275718.

**Graphic for Table of Contens:**

## High Transparency in the Structural Color Resin Films through Quasi-Amorphous Arrays of Colloidal Silica Nanospheres

Chun-Feng Lai,* Yu-Chi Wang, and Hsiang-Chih Hsu

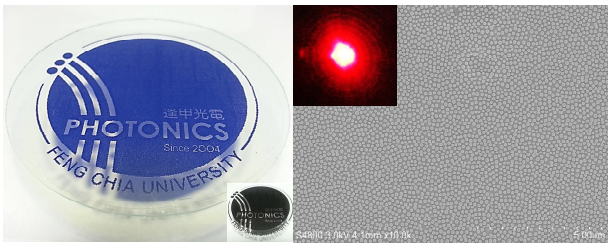


Novel quasi-amorphous structural color resin films are gigantic potential with highly transparent, uniform shining reflection color, and physical rigidity.